Isogenic organisms age at different rates due to critical-slowing-down of damage removal

Omer Karin[*1], Amit Agrawal[*1], Ziv Porat[2], Valery Krizhanovsky[#1], Uri Alon[#1]

[1]Dept. Molecular Cell Biology, Weizmann Institute of Science, Rehovot, Israel, 76100

[2]Dept. of Biological Services, Weizmann Institute of Science, Rehovot, Israel, 76100

[*]equal contribution

[#]corresponding authors (uri.alon@weizmann.ac.il, valery.krizhanovsky@weizmann.ac.il)

Abstract

Genetically-identical organisms age at different rates, but the reason for this is unclear. The rate of aging is due to the accumulation of damage, such as senescent cells (SnC) which are a major driver of aging in mammals, but the accumulation dynamics of SnC are unknown. Here, we combine theory and experiments in mice and find that SnC are rapidly produced and removed with a half-life of days in young mice. In old mice SnC half-life grows to weeks, because SnC saturate their own removal process. This saturation leads to persistent fluctuations known as critical-slowing-down: fluctuations are amplified to long-lasting differences in SnC between individuals at old ages. Rapid turnover with saturating removal is a general framework that may apply to any aging-related form of damage, and can quantitatively explain the demographic laws of mortality in worms, flies, mice and humans.

Introduction

As organisms age, intracellular damage accumulates, leading to the decline of physiological function. Even genetically identical organisms raised in the same conditions die at different times, suggesting a non-genetic stochastic component to mortality. This stochastic component has certain nearly universal features: in many species, including mice, nematodes, and humans, risk of death rises exponentially with age over several orders of magnitude, a relation known as the Gompertz law (*1*, *2*), showing a slowdown at very old ages. Experiments in nematodes show that many different lifespan-extending interventions have nearly identical survival curves when scaled by the mean lifespan, again suggesting that aging is controlled by a single stochastic process (*3*). Although much is known about cellular mechanisms of aging, the variation in aging rates between isogenic individuals, the Gompertz law and the scaling of survival curves have no explanation at the cellular level (Figure 1A).

To address this, we combine experiments and mathematical modelling to understand the stochastic accumulation of damage. We focus on a major driver of mammalian aging, the accumulation of senescent cells (SnC). SnC are damaged cells that stop dividing and secrete pro-inflammatory and anti-regenerative signals (*4*) (Figure 1B). They are identified using markers such as p16 and SA-β-Gal (*5*). SnC are produced in as a result of cellular stress, including DNA damage, damaged telomeres, and oxidative stress (*5*, *6*).

The number of SnC increases exponentially with age in mice and humans in many tissues (*5*, *7–12*). When they accumulate in the body, SnC impair tissue function and tissue regeneration, and cause chronic inflammation (*4*). Importantly, accumulation of SnC is causal for aging in mice: continuous targeted elimination of whole-body SnC increases mean lifespan by 25%, attenuates the age-related deterioration of heart, kidney, and fat, and delays cancer development (*13*). Similarly, removal of SnC causes improvement in diverse age-related conditions (*14–25*).

These studies indicate that SnC abundance is a critical variable underlying the aging process. We therefore asked whether the dynamics of SnC can explain the variation in aging rate between individuals, the Gompertz law of mortality and other population-level features. To address this question, we needed to determine the dynamics of SnC production and removal, which are currently unknown (*4*, *26*).

To understand the dynamics of SnC, we scanned a wide class of models of SnC dynamics, and, as described below, compared these models to longitudinal SnC trajectories (*7*) and direct SnC

induction experiments in mice (Figure 1C). The models describe production and removal of SnC. They differ from each other in the way that production and removal rates are affected by age and by SnC abundance (Figure 1C). The models describe all combinations of four possible mechanisms for accumulation of SnC: (i) SnC production rate can increase with age due accumulation of mutations (*27*), telomere damage and other forms of intracellular damage that trigger cellular senescence (*28*) (ii) SnC can catalyze their own production by paracrine and bystander effects (*29*), (iii) SnC removal can decrease with age due to age-related decline in immune surveillance functions (*30*), and (iv) high SnC levels can saturate their own immune surveillance mechanisms. This leads to a class of 16 different circuits (Figure 1C) with all combinations of these dependencies, in addition to basal parameters for production and removal. Each of these models has rate constants, which are currently uncharacterized.

To find which of the model mechanisms best describes SnC dynamics, we compared them to longitudinal data on SnC abundance in mice collected by Burd et al. (*7*). SnC abundance was measured using a luciferase reporter for the expression of $p16^{INK4a}$, a biomarker for senescent cells. Total body luminescence (TBL) was monitored every 8 weeks for 33 mice, from early age (8 weeks) to middle-late adulthood (80 weeks) (Figure 2A).

We tested how well each model describes the longitudinal SnC trajectories by finding the maximum likelihood parameters for each of the 16 models, adjusting for number of parameters (Supplementary Section 1 and Section 2). A principle emerges from this comparison: in order to capture the longitudinal dynamics, the mechanism must include saturation of removal rate, and have rapid turnover of SnC on the timescale of a few days in young mice. The simplest model that describes the data has only two interactions (Figure 2B): SnC production rate increases linearly with age, and SnC slow down their own removal rate by saturating the removal process, similar to saturation of an enzyme by its substrate. We call this the saturating removal model (SR model).

The SR model captures the accelerating rise of mean SnC abundance with age in the longitudinal data (Figure 2C), the increasing SnC variability between individuals (Figure 2D), and the SnC distributions between equal-aged individuals (Figure 2E) which are skewed to the right (Fig 2F). Importantly, the SR model also captures the fact that SnC fluctuations become more persistent with age, as evidenced by an increasing correlation between subsequent measurements (Figure 2G, $p<0.01$): individuals with higher (or lower) than average SnC levels stay higher (or lower) for longer periods with age. Models without saturation of removal show a poor overall fit (light-red line in Figure 2C).

The maximum likelihood parameters of the SR model provide quantitative predictions for SnC half-lives: (i) SnC turnover is rapid in young mice (3 month-old) with a half-life of about 5±1 day. (ii) Turnover rate slows down with age, so that SnC half-life is about 25±6 days at 22 months.

We tested these predictions using experiments in mice, by inducing the formation of senescent cells and analyzing their dynamics. To induce senescence in mice lungs we used intra-tracheal bleomycin administration (Figure 3A). Bleomycin is a DNA damaging agent that induces cellular senescence in the lung epithelium a few days after drug treatment (*5*, *31*).

We quantified the fraction of senescent lung epithelial cells at different time points following bleomycin administration (Figure 3A) using imaging flow cytometry. Epithelial SnC were defined as positive for a senescent cell marker (SA-β-Gal) and an epithelial marker (pan-Cytokeratin pCK). This cell population was also HMGB1 nuclear negative, as expected in senescent cells (*5*, *32*), and was previously shown (*5*) to be non-proliferative (negative Ki67 assay) (see Supplementary Section 3).

We first tested the prediction that turnover is rapid in young mice (Figure 3B). In 3 month-old mice, SnC decayed with a half-life of $\tau = 4.7$ days ($\tau^{-1} = 0.21 \pm 0.07\ days^{-1}$) and reached their baseline level within less than a month (Figure 3C). This result indicates that, as predicted, SnC levels in young mice are in a relatively fast dynamic balance of production and removal.

To test the prediction that removal slows with age (Figure 3B), we performed the bleomycin treatment in old mice (22 month-old). In these mice, the baseline level of SnC was about 5-fold higher than in young mice (Figure 3D). In the old mice, SnC decayed with a half-life of $\tau =$ 18 days ($\tau^{-1} = 0.055 \pm 0.035\ days^{-1}$), which was slower than that of young mice, as predicted (Figure 3B).

These turnover measurements quantitatively agreed with the predictions of the SR model (Figure 3D, Supplementary Section 4) with no additional fit. Notably, this agreement occurred despite the use of distinct SnC markers in the two data sets (SA-β-Gal in the bleomycin experiment vs. $p16^{INK4A}$-luciferase in the longitudinal experiment), indicating consistency between the measurement methods.

Our results suggest a core mechanism in which SnC accumulate because their production rate rises with age, and SnC saturate their own removal (Figure 4A). To understand how this mechanism works, consider the rate plot in Figure 4B, showing SnC production and removal curves as a function of SnC abundance. The crossing point of the curves is where production equals

removal, and is hence the SnC steady-state level. At young ages, production rate is low, resulting in a low steady-state SnC level (Figure 4A). Production rate rises with age, and SnC concentrations increasingly saturate the removal capacity (Figure 4AB), causing the SnC steady-state to shift to ever higher levels. This results in an accelerating rise of SnC abundance with age.

Most importantly, the saturation of removal amplifies small fluctuations in SnC, and results in long-lasting differences between individuals at old ages. To see this, note that young organisms have spare removal capacity, evidenced by large excess removal close to the steady-state point (shaded region Fig 4B). Old mice have much smaller spare removal capacity. Stochastic fluctuations take longer to remove in old mice, a phenomenon known as critical slowing down (*33*, *34*). This slowdown amplifies fluctuations and causes larger and more persistent variation between individuals with age (Figure 2G).

Inspired by these persistent individual differences in SnC, we asked whether SnC dynamics can explain the individual differences in mortality times, described by the Gompertz law (Kirkwood, 2015). To connect SnC dynamics and mortality, we need the relationship between SnC abundance and risk of death (*7*). The precise relationship is currently unknown. Since removing SnC from mice increases mean lifespan (*13*), and adding SnC to mice increases risk of death and causes age-related phenotypes (Xu et al., 2018), we reasoned that risk of death p should increase with SnC abundance, $p(X)$. For example, death can be modeled to occur when SnC exceed a threshold level X_C (*35*), representing a collapse of an organ system or a tipping point such as sepsis. We use this assumption to illustrate our approach, because it provides analytically solvable results. Other functions $p(X)$ provide similar conclusions (see Supplementary Section 2).

The SR model analytically provides the Gompertz law, including the observed deceleration of mortality rates at old ages (Figure 5, Supplementary Section 2). The model gives a good fit to the mouse mortality curve (Figure 5AB, see Supplementary Section 1 for details). Notably, it does so with parameters that agree with the present experimental half-life measurements and longitudinal SnC data (Supplementary Information 1). A good description of human mortality data, including the deceleration at old ages, is provided by the same parameters as in mice, except for a 60-fold slower increase in SnC production rate with age in the human parameter set (Figure 5C, Supplementary Section 5). This slower increase in SnC production rate can be due to improved DNA maintenance in humans compared to mice. We conclude that the SR mechanism for SnC dynamics provides a cellular mechanism for the variation in mortality between individuals (Figure 5D), based on the persistent noise in SnC levels caused by the saturation of removal rates.

The generality of the model suggests that it might apply to ageing dynamics in organisms without senescent cells, such as *Drosophila* and *C. elegans*, in which lifespan variation between isogenic organisms is well-studied (*3*, *36*). In these organisms, the present approach can be extended by considering X as cellular damage that saturates its own removal, such as protein damage that saturates proteostatic mechanisms (*37*).

For example, *Drosophila* shows rapid switches between hazard curves when transitioning from normal to lifespan-extending calorie restricted (CR) diets and vice versa (Fig 5D, inset). These switches are captured by the model when assuming that CR slows the rate of accumulation of damage η (Fig 5D and Supplementary Section 6). The rapid switches, on the timescale of two days, are due in the model to rapid damage turnover.

We further tested whether the SR model can explain the scaling of survival curves for *C. elegans* under different life-extending genetic, environmental and CR perturbations (*3*). These perturbations change lifespan by an order of magnitude, but the survival curves collapse on the same curve when age is scaled by mean lifespan (Figure 5E insets). We find that the SR model provides this scaling for perturbations that affect the damage accumulation rate η (Figure 5E). Interestingly, we predict loss of scaling when a perturbation affects other parameters such as removal rate β or noise ϵ (Supplementary Section 7), a prediction that may apply to exceptional perturbations such as the *eat-2* and *nuo-6* mutations, in which scaling is not found (Supplementary Section 6). In all cases, scaling cannot be explained without rapid turnover of damage. We conclude that the variation in aging rates between genetically identical flies and nematodes may stem from critical-slowing down of damage removal such as that described by the SR model.

The present results also bear on the use of drugs that eliminate SnC, known as senolytics (*38*). To reduce toxicity concerns, it is important to establish regimes of low dose and large inter-dose spacing. The model provides a rational basis for scheduling senolytic drug administrations. Specifically, treatment should start at old age, and can be as infrequent as the SnC turnover time (~month in old mice) and still be effective (Supplementary Section 8).

In summary, we propose a framework for understanding why individuals age at different rates, based on rapid turnover of damage with critical slowing down. In mice, this offers a quantitative link between cellular mechanisms and non-genetic variation in mortality based on persistent stochastic variability of SnC. Furthermore, because SnC are suggested to inhibit their own removal rate, drugs that remove senescent cells can have a double benefit – an immediate benefit from a reduced SnC load, and a longer-term benefit from increased SnC removal rate.

Similarly, interventions that increase removal capacity, for example by augmenting the immune surveillance of SnC, are predicted to be an effective approach to reduce SnC levels and increase the health-span.

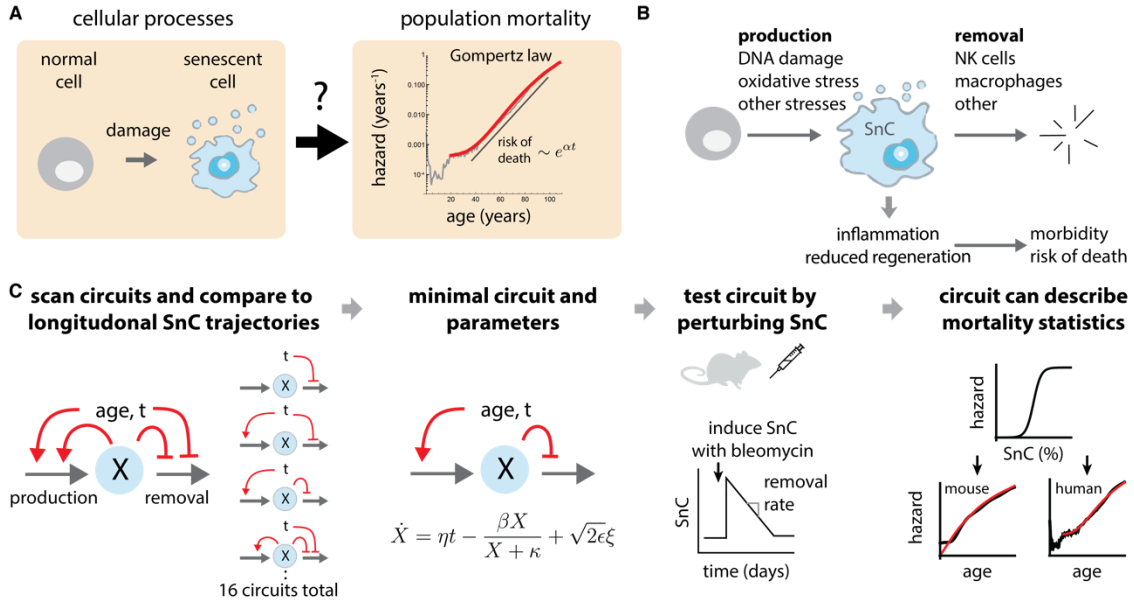

Figure 1. Approach for explaining the variation in aging rates between individuals in terms of damage accumulation. (A) The link between cellular damage mechanisms and the variation between individuals described by mortality statistics is unclear. (B) Many forms of damage lead to SnC production. SnC are cleared by immune mechanisms, and secrete factors that lead to morbidity. (C) We scan a wide class of models for SnC dynamics, and compare them to longitudinal SnC data and direct SnC perturbation experiments to establish a minimal model for SnC stochastic dynamics and its rate constants. We then show that this model and rate constants can explain the variation in mortality between individuals.

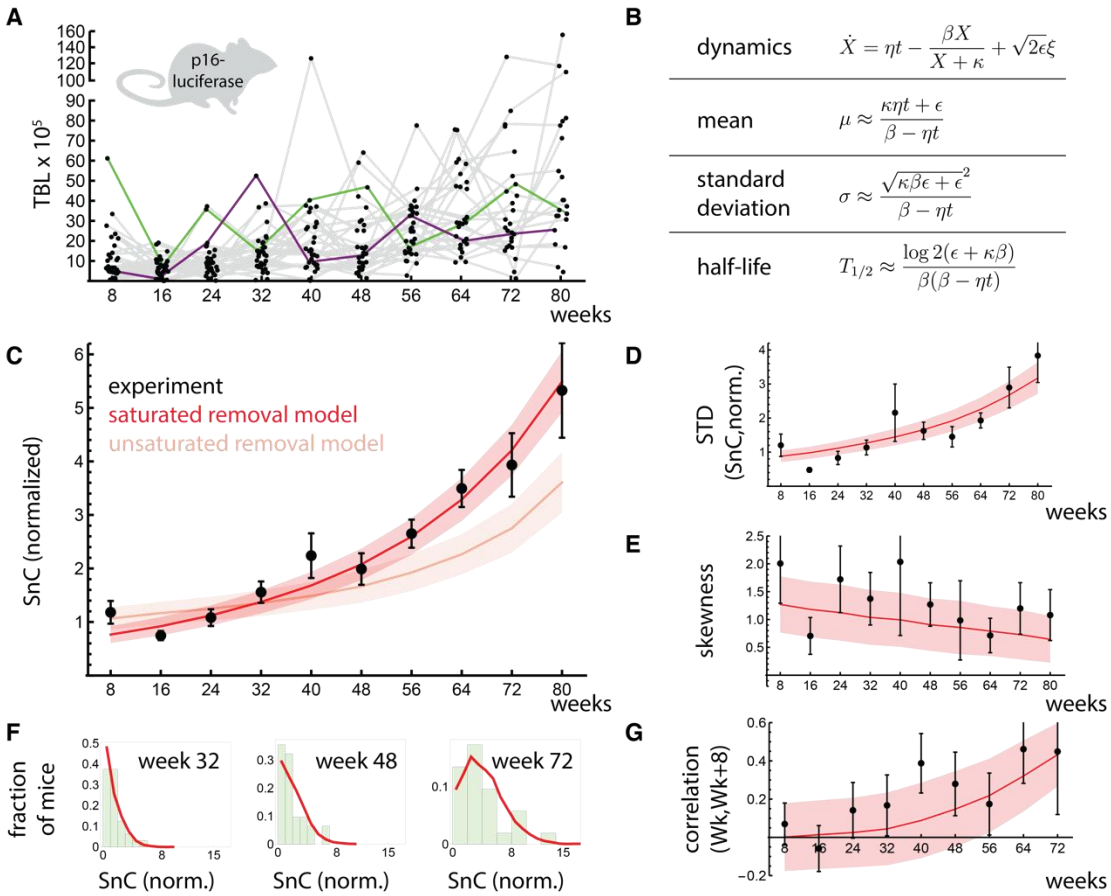

Figure 2. Saturated-removal (SR) model captures longitudinal SnC trajectories in mice. (A) Luminescence of p16-luciferase in mice. Grey lines connect data from the same individual mice. (B) SR model equations and their approximate analytical solutions. The SR model captures (C) the mean SnC abundance, (D) standard deviation of SnC abundance, (E) skewness and shape (F) of the distributions between equal-aged individuals, (G) correlation between subsequent measurements on the same individuals. TBL was normalized to give a mean abundance of 1 at young ages. Maximum likelihood parameters are: $\eta = 0.15\ day^{-1}year^{-1}$, $\beta = 0.27\ day^{-1}$, $\kappa = 1.1$, $\epsilon = 0.14\ day^{-1}$. Orange line: unsaturated removal (USR) model with best-fit parameters ($\frac{dX}{dt} = \eta_0 - (\beta_0 - \beta_1 t)X + \sqrt{2\epsilon}\xi,\ \eta_0 = 0,\ \beta_0 = 0.07\ day^{-1},\ \beta_1 = 0.044\ day^{-1}year^{-1},\ \epsilon = 0.22\ day^{-1}$). Mean and standard error (light red, orange regions) are from bootstrapping.

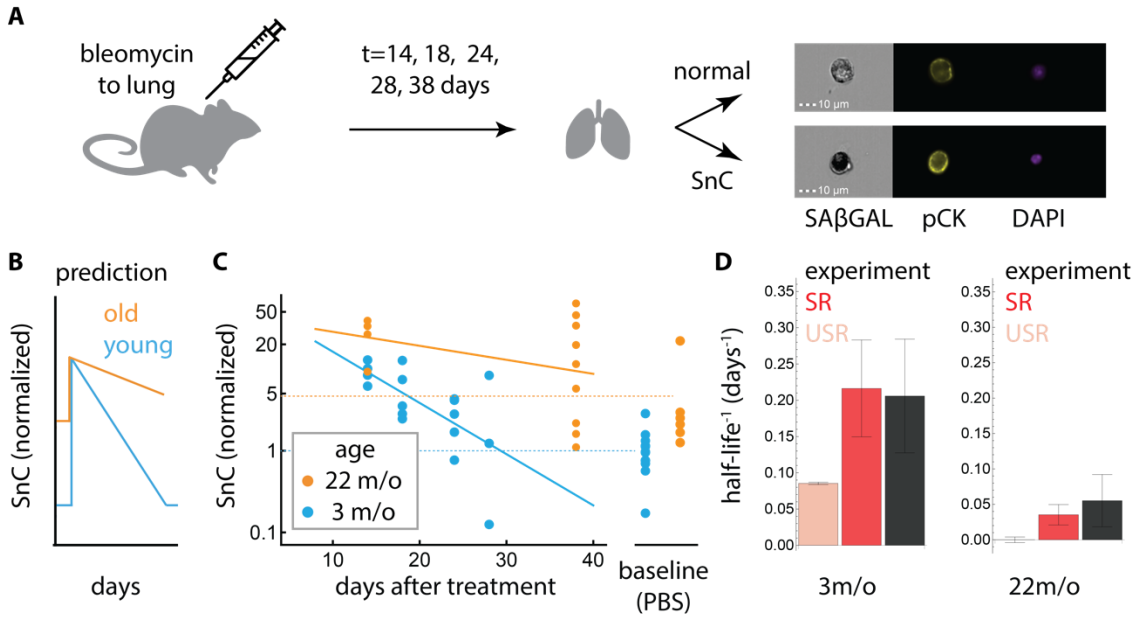

Figure 3. SnC half-life measurements in mice support SR model predictions. (A) Bleomycin or PBS was introduced by intratracheal installation to mice on day 0. Lungs were analyzed on the indicated days thereafter. Representative images of lung cells analyzed by imaging flow cytometry show how senescent epithelial cells were identified, using SA-β-Gal, Pan-Cytokeratin (pCK), and DAPI staining. SnC removal rate was estimated by fitting a log-linear model. (B) The SR model predicts that SnC rapidly return to baseline in young mice and that removal is slower in old mice. (C) Fraction of SnC in mice lung after treatment with bleomycin (1.5U/Kg). In young mice, SnC levels return to baseline with a half-life of about 5 days. In old mice, baseline SnC levels are about 5-fold higher, and SnC removal rate is slower than in young mice ($p=0.038$). (D) SnC removal rates (half-life^{-1}) for young and old mice (mean and SE, black) agree with the SR model predictions (red, mean and SE were calculated by bootstrapping, see Methods). The best-fit model without saturated removal (USR) shows a poor prediction (orange).

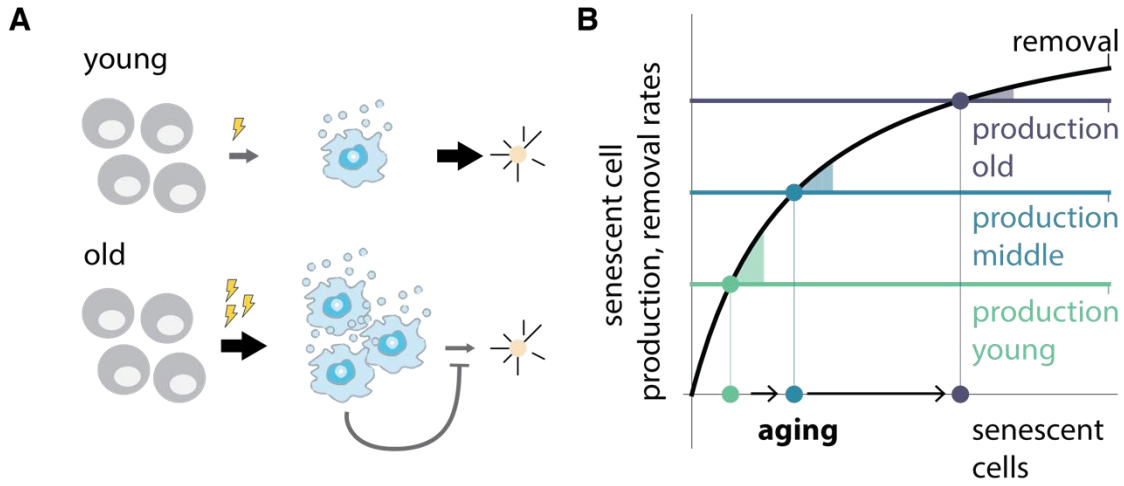

Figure 4. Saturating removal and increasing production lead to accelerated SnC abundance with age and persistent SnC fluctuations. (A) With age, production rate increases, SnC levels rise and increasingly saturate their own removal mechanism, further amplifying their rate of increase. (B) Removal and production rates plotted as a function of SnC abundance. Steady-state occurs when production and removal curves cross (dots). As production rises, SnC levels accelerate to higher abundance. At old ages, the spare capacity for removal (the distance between production and removal curves, shaded regions) shrinks, so that SnC perturbations last longer, leading to persistent fluctuations. These fluctuations cause non-genetic variations between individuals that last for long times.

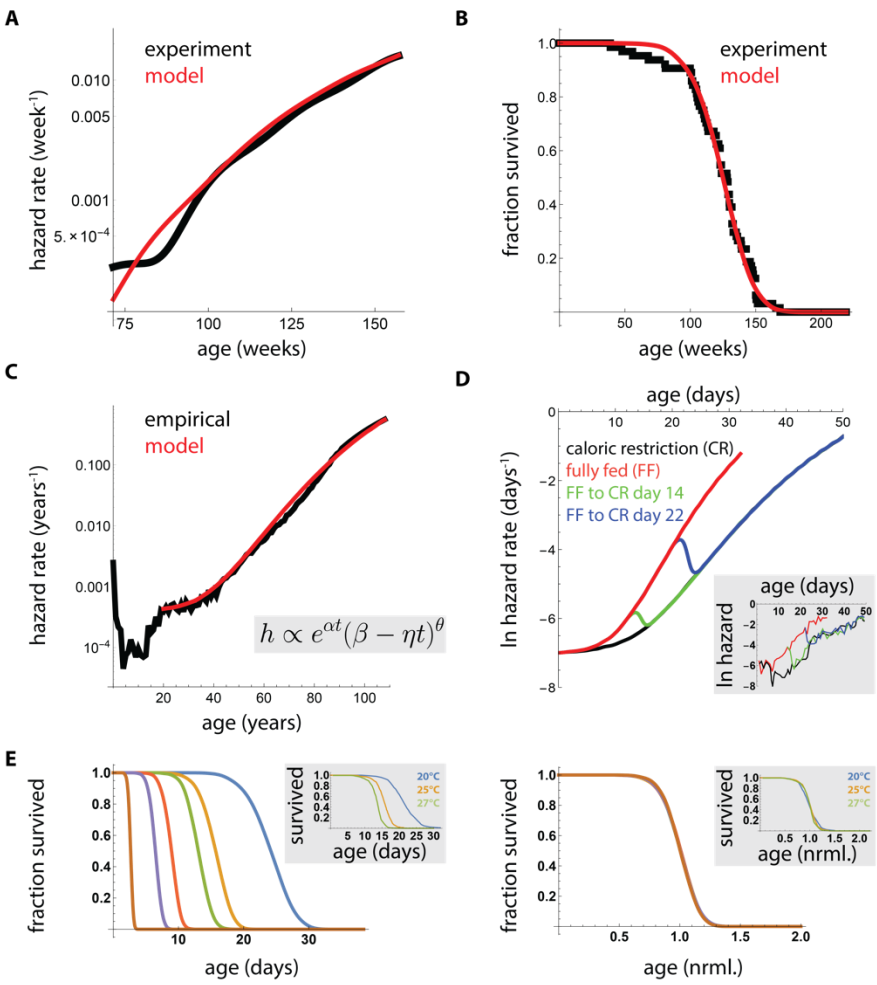

Figure 5. Saturated removal model can explain the variability in mortality between individuals. (A,B) Mouse mortality (C57BL/6J mice obtained from the Mouse Phenome Database (*39*), black line) is well fit by the SR model (red line) with parameters consistent with the data of Figures 1, 2, with death when SnC exceed a threshold X_c (see Supplementary Information 1 for parameters). (C) The model with added age-independent extrinsic mortality ($0.4 \cdot 10^{-3} year^{-1}$) (red) matches human mortality statistics (*40*) (black). Inset: approximate analytical solution for mortality in the SR model shows the Gompertz law and deceleration at old ages. (D) When fully fed *Drosophila* transition to caloric restriction (CR), mortality shifts within 2 days to the level of flies on CR throughout their lifespan (inset) (*36*). This is captured by the SR model with rapid damage turnover, with CR modeled by a decrease in damage production rate η (see Supplementary Section 6). (E) *C. elegans* raised at different temperatures vary by an order of magnitude in lifespan, but survival curves collapse on a single curve when time is scaled by mean lifespan (inset –data from (*3*)). The SR model provides scaling for perturbations that affect η, but not other parameters

(see Supplementary Information 7 and Methods for similar results on other lifespan extending perturbations).

Acknowledgments

U.A. is the incumbent of the Abisch-Frenkel chair. O.K. is an Azrieli Fellow. This work was supported by grants to V.K. from the European Research Council under the European Union's FP7 and H2020 Programs and the Israel Science Foundation.

References

1. B. Gompertz, On the Nature of the Function Expressive of the Law of Human Mortality, and on a New Mode of Determining the Value of Life Contingencies. *Philos. Trans. R. Soc. Lond.* **115**, 513–583 (1825).

2. T. B. L. Kirkwood, Deciphering death: a commentary on Gompertz (1825) 'On the nature of the function expressive of the law of human mortality, and on a new mode of determining the value of life contingencies.' *Phil Trans R Soc B.* **370**, 20140379 (2015).

3. N. Stroustrup *et al.*, The temporal scaling of Caenorhabditis elegans ageing. *Nature*. **530**, 103–107 (2016).

4. S. He, N. E. Sharpless, Senescence in Health and Disease. *Cell*. **169**, 1000–1011 (2017).

5. A. Biran *et al.*, Quantitative identification of senescent cells in aging and disease. *Aging Cell*. **16**, 661–671 (2017).

6. D. Muñoz-Espín, M. Serrano, Cellular senescence: from physiology to pathology. *Nat. Rev. Mol. Cell Biol.* **15**, 482–496 (2014).

7. C. E. Burd *et al.*, Monitoring Tumorigenesis and Senescence In Vivo with a p16INK4a-Luciferase Model. *Cell*. **152**, 340–351 (2013).

8. Y. Liu *et al.*, Expression of p16INK4a in peripheral blood T-cells is a biomarker of human aging. *Aging Cell*. **8**, 439–448 (2009).

9. A. Melk *et al.*, Expression of p16INK4a and other cell cycle regulator and senescence associated genes in aging human kidney. *Kidney Int.* **65**, 510–520 (2004).

10. T. Sofue *et al.*, Tubular Cell Senescence in the Donated Kidney Predicts Allograft Function, but Not Donor Remnant Kidney Function, in Living Donor Kidney Transplantation. *Am. J. Nephrol.* **47**, 8–17 (2018).

11. U. Herbig, M. Ferreira, L. Condel, D. Carey, J. M. Sedivy, Cellular senescence in aging primates. *Science*. **311**, 1257 (2006).

12. S. Zhou *et al.*, Age-related intrinsic changes in human bone-marrow-derived mesenchymal stem cells and their differentiation to osteoblasts. *Aging Cell*. **7**, 335–343 (2008).

13. D. J. Baker *et al.*, Naturally occurring p16(Ink4a)-positive cells shorten healthy lifespan. *Nature*. **530**, 184–189 (2016).

14. M. P. Baar *et al.*, Targeted Apoptosis of Senescent Cells Restores Tissue Homeostasis in Response to Chemotoxicity and Aging. *Cell*. **169**, 132-147.e16 (2017).

15. J. Chang *et al.*, Clearance of senescent cells by ABT263 rejuvenates aged hematopoietic stem cells in mice. *Nat. Med.* **22**, 78–83 (2016).

16. R. Yosef *et al.*, Directed elimination of senescent cells by inhibition of BCL-W and BCL-XL. *Nat. Commun.* **7**, 11190 (2016).

17. M. Xu *et al.*, Targeting senescent cells enhances adipogenesis and metabolic function in old age. *eLife*. **4**, e12997 (2015).

18. C. M. Roos *et al.*, Chronic senolytic treatment alleviates established vasomotor dysfunction in aged or atherosclerotic mice. *Aging Cell*. **15**, 973–977 (2016).

19. B. G. Childs *et al.*, Senescent intimal foam cells are deleterious at all stages of atherosclerosis. *Science*. **354**, 472–477 (2016).

20. M. J. Schafer *et al.*, Cellular senescence mediates fibrotic pulmonary disease. *Nat. Commun.* **8**, 14532 (2017).

21. M. Ogrodnik *et al.*, Cellular senescence drives age-dependent hepatic steatosis. *Nat. Commun.* **8**, 15691 (2017).

22. O. H. Jeon *et al.*, Local clearance of senescent cells attenuates the development of post-traumatic osteoarthritis and creates a pro-regenerative environment. *Nat. Med.* **23**, 775–781 (2017).

23. J. Krishnamurthy *et al.*, p16INK4a induces an age-dependent decline in islet regenerative potential. *Nature*. **443**, 453–457 (2006).

24. A. Sagiv *et al.*, p53 in Bronchial Club Cells Facilitates Chronic Lung Inflammation by Promoting Senescence. *Cell Rep.* **22**, 3468–3479 (2018).

25. M. Xu *et al.*, Senolytics improve physical function and increase lifespan in old age. *Nat. Med.* (2018).

26. C. López-Otín, M. A. Blasco, L. Partridge, M. Serrano, G. Kroemer, The Hallmarks of Aging. *Cell*. **153**, 1194–1217 (2013).

27. M. Enge *et al.*, Single-Cell Analysis of Human Pancreas Reveals Transcriptional Signatures of Aging and Somatic Mutation Patterns. *Cell*. **171**, 321-330.e14 (2017).

28. F. d'Adda di Fagagna, Living on a break: cellular senescence as a DNA-damage response. *Nat. Rev. Cancer*. **8**, 512–522 (2008).

29. J. C. Acosta *et al.*, A complex secretory program orchestrated by the inflammasome controls paracrine senescence. *Nat. Cell Biol.* **15**, 978–990 (2013).

30. D. Aw, A. B. Silva, D. B. Palmer, Immunosenescence: emerging challenges for an ageing population. *Immunology*. **120**, 435–446 (2007).

31. K. Aoshiba, T. Tsuji, A. Nagai, Bleomycin induces cellular senescence in alveolar epithelial cells. *Eur. Respir. J.* **22**, 436–443 (2003).

32. A. R. Davalos *et al.*, p53-dependent release of Alarmin HMGB1 is a central mediator of senescent phenotypes. *J. Cell Biol.* **201**, 613–629 (2013).

33. D. Podolskiy *et al.*, Critical dynamics of gene networks is a mechanism behind ageing and Gompertz law. *ArXiv150204307 Phys. Q-Bio* (2015) (available at http://arxiv.org/abs/1502.04307).

34. M. Scheffer *et al.*, Early-warning signals for critical transitions. *Nature*. **461**, 53–59 (2009).

35. J. S. Weitz, H. B. Fraser, Explaining mortality rate plateaus. *Proc. Natl. Acad. Sci.* **98**, 15383–15386 (2001).

36. W. Mair, P. Goymer, S. D. Pletcher, L. Partridge, Demography of dietary restriction and death in Drosophila. *Science*. **301**, 1731–1733 (2003).

37. E. A. Kikis, T. Gidalevitz, R. I. Morimoto, in *Protein Metabolism and Homeostasis in Aging*, N. Tavernarakis, Ed. (Springer US, Boston, MA, 2010; http://link.springer.com/10.1007/978-1-4419-7002-2_11), vol. 694, pp. 138–159.

38. Y. Ovadya, V. Krizhanovsky, Strategies targeting cellular senescence. *J. Clin. Invest.* **128**, 1247–1254 (2018).

39. S. C. Grubb, C. J. Bult, M. A. Bogue, Mouse Phenome Database. *Nucleic Acids Res.* **42**, D825–D834 (2014).

40. M. Barbieri *et al.*, Data Resource Profile: The Human Mortality Database (HMD). *Int. J. Epidemiol.* **44**, 1549–1556 (2015).